BioChip Journal (2021) 15:381–395
https://doi.org/10.1007/s13206-021-00038-9

ORIGINAL ARTICLE

Zinc-Finger-Protein-Based Microfluidic Electrophoretic Mobility Reversal Assay for Quantitative Double-Stranded DNA Analysis

Nebiyu Getachew Arega[1] · Whitney N. Heard[2] · Nguyen Anh Nhung Tran[3] · Sukyo Jung[3] · Jianyun Meng[1] · Minsub Chung[3] · Moon-Soo Kim[2] · Dohyun Kim[1]

Received: 13 September 2021 / Revised: 22 October 2021 / Accepted: 25 October 2021 / Published online: 10 November 2021

Abstract
We report for the first time a microfluidic electrophoretic mobility reversal assay (MEMRA) for double-stranded DNA (dsDNA) detection using zinc-finger proteins (ZFPs) and a polyacrylamide-gel (PAG) sieving matrix. Microfluidic DNA analysis was actively studied because of its importance in biology and medicine. Most microfluidic DNA detection techniques rely on time-consuming denaturation and hybridization processes. To address this limitation, ZFP was employed as a novel affinity probe, which directly binds to a specific sequence of dsDNA without denaturation and renaturation. A mildly alkaline electrophoresis buffer (pH 8.6) was used for our MEMRA, instead of a strongly alkaline buffer (pH 10.75) for separating the ZFP–dsDNA complex from interfering species. At pH 8.6, the mobility of ZFP was reversed upon binding with dsDNA (complex pI = ~5.33), and unbound ZFP (pI = ~9.3) was excluded from loading. Therefore, the ZFP–dsDNA complex was detected without zone interferences. Furthermore, nonspecific interactions and band dispersion, observed in strongly alkaline buffer, were effectively mitigated in the MEMRA. The ZFP–dsDNA complex was fully separated (separation resolution ≥ 2.0) and detected rapidly (12–15 s at a separation distance of 160–240 μm) using on-chip photopatterned 3–16%T discontinuous PAG. The MEMRA performance was excellent, providing a detection limit of 50 pM and a detection range of 100 pM–500 nM for *seb* (*Staphylococcus* enterotoxin B) gene dsDNA oligonucleotides. We expect that our ZFP-based MEMRA will find broad utility in biology and medicine where the rapid, specific, and quantitative detection of dsDNA is of paramount importance.

Keywords Microchip electrophoresis · Electrophoretic homogeneous affinity assay · Double-stranded DNA analysis · *Staphylococcus aureus* · Zinc-finger protein

1 Introduction

The electrophoretic mobility shift assay (EMSA) is an electrokinetics-based analytical technique relying on the mobility difference between a target analyte and its complex with an appropriate binding partner [1–3]. The method can extract important kinetic information regarding protein–protein, protein–DNA (RNA), protein–carbohydrate, protein–small molecule, DNA–small molecule, small molecule–small molecule interactions, and so forth, by measuring mobility shifts upon binding [4–6]. The homogeneous electrophoresis affinity assay (HEAA), a type of EMSA, can provide quantitative information about a target analyte by determining the amount of a complex peak separated from an unbound probe peak. The HEAA possesses the following advantages over conventional solid-support-based heterogeneous assays: (1) electrophoresis is a molecular separation technique that allows for unbound probe, unassociated target molecules, and other interfering species in the sample matrix to be spatially or temporarily separated without tedious multiple wash steps, usually required for heterogeneous assay [3]; (2) for capillary [3] and microchip formats [7], only minute amounts of sample and reagents are consumed as the channel or capillary diameter is typically ~100 μm or less; (3) liquid-phase homogeneous reactions enable faster

✉ Dohyun Kim
dohyun.kim@mju.ac.kr

[1] Department of Mechanical Engineering, Myongji University, Yongin-si, Gyeonggi-do 17508, South Korea

[2] Department of Chemistry, Western Kentucky University, Bowling Green, KY 42101, USA

[3] Department of Chemical Engineering, Hongik University, Mapo-gu, Seoul 04066, South Korea

diffusion between free analytes and probes than diffusion to probes immobilized on a solid support [3]; (4) rapid separation (10 s of seconds to minutes) [3, 7] and parallelized separation in a capillary bundle or an array of microfluidic channels allow for high throughput which can be comparable to that of multiwell-plate-based heterogeneous assays [2, 8, 9]; and lastly (5) sub-nM detection limits can be achieved using fluorescence-conjugated probes and a laser-induced fluorescence (LIF) system [10].

Owing to the aforementioned advantages, HEAA based on antibody affinity probes has been studied since the 1990s in capillary [11, 12] and microchip formats [13, 14]. Both direct immunoassays (labeled probe antibody binds directly to a target analyte to generate a measurable signal) [12, 14] and competitive immunoassays (labeled and unlabeled target molecules compete for binding with unlabeled antibody) [11, 13] have been demonstrated. The competitive format is generally believed to be superior owing to larger mobility shifts of complexes [3]. Common analytes for the HEAA immunoassay include proteins [7, 8, 14–16], hormones [11–13, 17], drugs [14], and toxins [18].

A large body of literature is based on EMSA-derived information regarding DNA–protein interactions [4–6, 19–22] owing to their importance in the molecular biology of gene regulation. The detection and analysis of DNA are also crucial for various other applications [23, 24], including microbiology [25], pharmacology [26], forensic science [27], genotyping [28, 29], gene-expression study [30], genetic-disease diagnosis [31], and pathogen detection [32–35]. Therefore, the development of a rapid, sensitive, and specific microfluidic assay for DNA analysis is of significant interest [36, 37]. However, a surprisingly small number of attempts have been made to quantify DNA using the HEAA [23, 38]. Huber et al. electrokinetically separated 20-mer single-stranded DNA (ssDNA) and its hybridization complex using a microfluidic device equipped with a nanofabricated molecular sieve to detect the target sequence and quantify the kinetic parameters [23]. The mobility shift of a target ssDNA was detected after hybridization with fluorescence-labeled ssDNA probes. However, hybridization with complementary ssDNA probes requires time-consuming denaturation and subsequent hybridization steps, as well as a separate heating instrument [39, 40]. Moreover, the formation of secondary structures, such as a hairpin structure, in ssDNA probes may affect the binding efficiency and consequently lower the analytical sensitivity [41].

Herein, for the first time, we propose the use of zinc-finger protein (ZFP), which is a nucleic-acid-recognizing protein motif [42], as a novel affinity probe for quantifying double-stranded DNA (dsDNA) in a direct microfluidic polyacrylamide-gel HEAA format (Fig. 1). An engineered ZFP can directly bind to specific sequences of dsDNA oligonucleotides, mitigating tedious denaturation and subsequent renaturation processes, as presented in Fig. 1a [39]. A zinc finger (ZF) is one of the most common types of DNA-binding domains found in eukaryotes. A Cys2-His2 (C2H2) ZF domain contains two cysteine and two histidine residues that coordinate a zinc ion, stabilizing the protein fold along with hydrophobic interactions [43]. Each domain folds into a ββα structure and contains 30 amino acids [43]. The C2H2 ZF domain recognizes three to four DNA nucleotides, and multiple fingers can be linked together in a tandem array to recognize any extended DNA sequences. For example, 6 finger proteins can bind to 18 base pairs (bps) of a specific DNA sequence, which is long enough to specify a unique site in the genome [44–46]. Previously, an individual ZF module has been identified to recognize any of the 64 possible 3-bp subsites using combinatory mutagenesis and selection methods [45–47]. Predefined ZF modules can be assembled to form multi-finger proteins to recognize any desired DNA

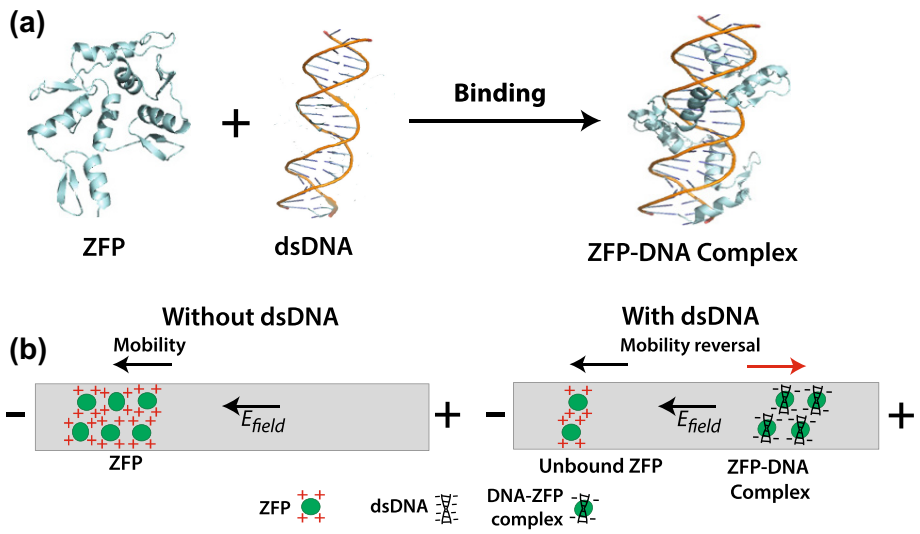

Fig. 1 Concept of the microfluidic electrophoretic mobility reversal assay (MEMRA). **a** Zinc-finger protein (ZFP), a DNA-binding protein motif, binds to double-stranded DNA (dsDNA) without denaturation and subsequent renaturation. **b** ZFP mobility, initially positive in a mildly alkaline electrophoresis buffer, such as tris–glycine buffer, is reversed upon binding with dsDNA oligonucleotides, migrating in the opposite direction under an electric field

sequence through a modular assembly approach [48]. Therefore, ZF modules provide a versatile and powerful scaffold to engineer custom-designed DNA-binding proteins that can recognize specific sequences, depending on target DNA.

We opted for the direct HEAA format over the competitive format, because a larger dynamic range can be achieved [2], and the assay can be integrated with signal enhancing techniques, such as chemiluminescence [49]. Moreover, the direct HEAA procedure is simpler as only prelabeled probes are required, whereas both labeled targets and unlabeled probes need to be co-incubated with unlabeled targets in the competitive format. The uniqueness of our microfluidic HEAA is mobility reversal of the ZFP probe upon binding with a target DNA. Our zinc finger is positively charged in tris–glycine buffer (pH 8.6), because it is an alkaline protein (pI = ~9.3). However, upon binding with strongly negative dsDNA oligonucleotides, the polarity of the ZFP–DNA complex reverses becoming negative, as displayed in Fig. 1b. Because of this mobility reversal, unbound ZFP cannot be loaded into a microfluidic device, whereas the ZFP–DNA complex, unbound DNA, and internal standard can be properly loaded under an appropriate electric-field condition. The benefits of our microfluidic electrophoretic mobility reversal assay (MEMRA) are two-fold. First, multiple HEAA issues associated with the use of strongly alkaline buffers (i.e., alkaline electrophoresis) including nonspecific protein interactions, low binding affinity, polyacrylamide gel hydrolysis, and incomplete polymerization, can be mitigated [16, 50, 51]. Second, unbound ZFP is completely excluded from the microchannel. Therefore, low-resolution separation with zone interference, a common drawback of the direct format, can be avoided. We chose the name MEMRA to signify the reversal of probe mobility upon binding and differentiate it from the EMSA.

In addition, we adopted photopatterned polyacrylamide gel (PAG) to further surmount the limitation of a small mobility shift observed in the direct HEAA [3, 23]. Originally adopted in a microfluidic format by Brahmasandra et al. [52], the PAG, crosslinked locally inside a microfluidic channel, functions as a molecular sieve and anti-convection medium. The PAG also greatly enhances the electrophoresis performance. As in some slab-gel electrophoresis cases [53], a PAG with discontinuous pore size (or discontinuous monomer concentration) minimizes initial peak width by stacking a sample plug at the discontinuity interface. Therefore, the discontinuous PAG system improves separation resolution, completes separation within a shorter time, and reduces overall device size [7, 16, 51, 54]. We employed a discontinuous PAG comprising 3%T loading gel and 16%T separation gel fabricated in a double-T junction microfluidic device to improve separation resolution.

To evaluate our ZEP-based MEMRA, the *seb* gene encoding for *Staphylococcus* enterotoxin B (SEB) was analyzed. *Staphylococcus aureus* (*S. aureus*) is a common human pathogen present in the nasal passages, skin, face, and wounds. It is a causative agent of various infections, including skin and respiratory infections [55]. Enterotoxigenic *S. aureus* is also the common cause of food poisoning, resulting in symptoms such as vomiting, diarrhea, abdominal cramps, fever, and dehydration [56, 57]. There are eight major types of enterotoxins produced by *S. aureus*, and they are proteins of low molecular masses (27–34 kDa). Among them, SEB is stable and resistant to pepsin under normal stomach conditions [56]. Although not life-threatening, SEB can incapacitate humans for several days to weeks. The presence of SEB in food samples is commonly diagnosed using a conventional culture method, but it is time-consuming, requiring days to weeks to obtain results. Therefore, the "golden time" for preventing outbreaks would elapse [58]. A rapid, specific, and sensitive method of enterotoxin detection is crucial for the timely prevention of bacterial outbreaks. PCR with agarose electrophoresis sometimes takes up to 8 h to complete. Even real-time PCR can take 1.5 h just for a run in addition to sample preparation [32]. Our MEMRA has the potential to deliver a rapid, miniaturized, sensitive gene analysis platform, incorporated with photomultiplier tube (PMT) detection. Therefore, foodborne outbreaks could be prevented in a timely manner.

2 Materials and Methods

2.1 Reagents and Consumables

Reagents for PAG and linear acrylamide coatings, dimethyl sulfoxide (DMSO), glacial acetic acid, 3-(trimethoxysilyl) propyl methacrylate, 30% acrylamide/bis-acrylamide solution (29:1), and 40% acrylamide solution were acquired from Sigma (St. Louis, MO, USA). The photoinitiator, 2,2-azobis [2-methyl-*N*-(2-hydroxyethyl) propionamide] was sourced from Wako Chemicals (Osaka, Japan), and methanol was obtained from Samchun Chemicals (Seoul, South Korea). For isoelectric focusing (IEF), hydroxyethyl cellulose (HEC), carrier ampholyte (Pharmalyte pH 3–10), and fluorescent pI markers (5.2, 5.9, 8.1, and 9.5) were purchased from Sigma; 1 N sodium hydroxide (NaOH) was obtained from Daejung Chemicals (Siheung, South Korea); 70 mM phosphoric acid (H_3PO_4, 70 mM) was supplied by BioRAD Laboratories (Hercules, CA, USA). For MEMRA development, $ZnCl_2$, $MgCl_2$, KCl, tris(hydroxymethyl) aminomethane (Tris) base, *N*-cyclohexyl-3-aminopropanesulfonic acid (CAPS), 3-[(3-cholamidopropyl) dimethylammonio]-1-propanesulfonate hydrate (CHAPS), Nonidet p-40 (NP40), Tween 20, and dithiothreitol (DTT) were obtained from Sigma; 10 × Tris–borate-EDTA (TBE) buffer and 10 × Tris–glycine buffer (TG) were purchased

from BioRAD. Protein internal standards bovine-serum albumin (BSA*) and ovalbumin (OVA*), pre-conjugated with Alexa Fluor 488 (AF488), were purchased from Invitrogen (Carlsbad, CA, USA). AF488 protein labeling kits from Invitrogen and Bio-spin P6 gel column from BioRAD were used for fluorescence conjugation of ZFP. The *seb* gene labeled with Cy5 at the 5' end was purchased from Integrated DNA Technologies (Coralville, IA, USA). All consumables that came into contact with DNA, including pipette tips and microcentrifuge tubes, and DI water were sterilized in an autoclave (HK-AC100, Hankuk S&I, Hwaseong, South Korea) under the sterilization conditions of 15 psi, 121 °C for 15 min to prevent nuclease reaction.

2.2 Preparation of Target DNA Oligonucleotides

Single-stranded target DNA oligonucleotides labeled with Cy5 were purchased from Integrated DNA Technologies. Target dsDNA oligonucleotides were prepared by heating at 95 °C for 10 min and then slowly cooling down to ambient temperature to form hairpins containing a four-thymidine loop. The sequence of the *seb* gene (SEB-435) oligonucleotide is provided below. The recognition site is highlighted in bold.

5′(Cy5)-GAC GGT GTG ACC GAG CAT GAT **GGA AAT CAA ATA GAT AAA** CCC TTTT GGG **TTT ATC TAT TTG ATT TCC** ATC ATG CTC GGT CAC ACC GTC-3′

2.3 Construction, Expression, and Purification of ZFPs

A ZFP was engineered to detect the *seb* gene encoding for SEB in *S. aureus* using the modular assembly method [59]. The DNA-coding region for the ZFP was commercially synthesized by Bio Basic (Amherst, NY, USA). The gene was inserted into a pMAL vector after a maltose-binding protein (MBP). This enables bacterial expression of the fusion ZFP protein with an N-terminal MBP as a purification tag.

The pMAL-ZFP_SEB435 was expressed in *E.coli* BL21. Cells were grown overnight at 37 °C in 5 mL of LB media containing ampicillin and then scaled up to 300 mL of LB media. When the optical density reached 0.4–0.6, cells were cooled to 23 °C for 20 h. Cells were pelleted and resuspended in Zinc Buffer A (ZBA; 100 mM Tris base + 90 mM KCl + 1 mM $MgCl_2$ + 100 mM $ZnCl_2$ at pH 7.5) including 5 mM DTT [39, 60]. After sonication and centrifugation, the supernatant was applied to an amylose-resin column pre-equilibrated with ZBA buffer with 5 mM DTT, and then washed with 2 M NaCl + ZBA and ZBA + 5 mM DTT. The MBP–ZFP was eluted in the buffer containing ZBA + 10 mM maltose + 5 mM DTT. Protein concentration was determined by measuring the absorbance at 280 nm on a microplate reader (Multiskan™ GO Microplate Spectrophotometer, Thermo Fisher Scientific, Waltham, MA, USA), and purity was assessed with polyacrylamide gel electrophoresis with sodium dodecyl sulfate (SDS–PAGE).

Because we found that the MBP–ZFP_SEB435 fusion protein was auto-cleaved and yielded multiple bands in SDS-PAGE, the MBP tag was removed to avoid assay complication (i.e., zone interference). The fusion protein was cleaved by Factor Xa in reaction buffer (20 mM Tris–HCl + 100 mM NaCl + 2 mM $CaCl_2$ at pH 7.0). The reaction mixture containing MBP (42.5 kDa), ZFP (19.5 kDa), and unreacted MBP–ZFP (62 kDa) was purified using affinity chromatography with amylose resin as described above to remove all forms of MBP. To eliminate MBP completely, the eluted protein was purified again employing fast-protein liquid chromatography (FPLC, GE Healthcare, Buckinghamshire, UK) with a size-exclusion column (Superdex™ 200 Increase 10/300 GL, GE Healthcare) in 25 mM Tris + 150 mM NaCl buffer (pH 7.4). Because the molecular weight of ZFP is almost two times smaller than that of MBP, ZFP was eluted much later than MBP. The buffer was exchanged to ZBA buffer (pH 7.5) using a Vivaspin 20 centrifugal concentrator (5 kDa cutoff, Sigma). Purified protein was stored in a ZBA + 5 mM DTT solution at 4 °C until use.

2.4 Fluorescence Conjugation of ZFP

The ZFP was fluorescence-labeled with AF488 dye, as per the manufacturer's protocol. Briefly, the ZFP was incubated overnight with the AF488 dye in DMSO at 4 °C. Sodium bicarbonate solution (1 M) was used to adjust the pH of the reaction mixture to pH 9 for effective labeling. Afterward, the labeled protein was separated from unbound dye using a Bio-spin 6 column, previously buffer-exchanged with 1 × TG with 0.1 mM $ZnCl_2$ (pH 8.6). Finally, the concentration of ZFP* (*symbol denotes labeled with fluorescence), and the degree of labeling were determined spectroscopically at 280 and 495 nm using a spectrophotometer (NanoPhotometer, Implen, Munich, Germany). ZFP* was stored at 4 °C until further use.

2.5 p*I*-Point Measurement of ZFP

Isoelectric points (p*I*) of ZFP* and ZFP*–DNA complex were measured to evaluate if mobility reversal is possible upon forming a complex and to select an adequate electrophoresis buffer (running buffer) for the MEMRA. Isoelectric focusing was performed in a microfluidic format (μIEF). A glass microfluidic chip with an isotropically etched straight channel of 50 μm nominal width, 12 mm length, and 50 μm depth (IMT, Greifensee, Switzerland) was cleaned with 1 N NaOH for 5 min, followed by rinsing with DI water. The channel was then flushed with methanol for 5 min and dried

by suction. Degassed silane solution, containing a 2:2:3:3 (v/v/v/v) mixture of glacial acetic acid, 3-(trimethoxysilyl) propyl methacrylate, methanol and DI water, was then loaded into the channel using capillary action. The silane solution was incubated inside the microchannel for 30 min for assembling a silane monolayer, followed by cleaning with methanol for 30 min. Finally, the microchannel was dried by suction. The silane monolayer enhances covalent bonding between the glass surface and acrylamide. The inner surface of the microchannel was coated with 6%T linear acrylamide by introducing 6%T precursor solution and flood exposure for 10 min at 6 mW/cm^2 using a custom-made UV exposure system, equipped with a collimated UV LED lamp (M365LP1-C1, Thorlabs, Newton, NJ, USA). The UV exposure system was cooled with fans to maintain a constant temperature in the exposure region, because elevated temperatures generated unwanted bubbles. The linear-acrylamide precursor solution consisted of 6%T acrylamide and 0.2% (w/v) VA-086 photoinitiator.

ZFP* incubated with DNA in 0.1% NP40 + 1 mM DTT + 1 × TG for 2 h, and four fluorescent p*I* markers, 5.2 (3.33 µg/ml), 5.9 (6.66 µg/ml), 8.7 (3.33 µg/ml), and 9.5 (25 µg/ml), were added to a separation matrix containing 6.25% (v/v) carrier ampholyte, 7.2% (w/v) HEC, and 5% (w/v) CHAPS. $ZnCl_2$ was not added to the separation matrix due to high current and poor focusing results. After the resulting mixture was loaded into the microchannel, anolyte (17.5 mM H_3PO_4 + 6% HEC) and catholyte (50 mM NaOH + 6% HEC) were placed on the anode and cathode reservoirs (made out of cut 200-µL pipette tips), respectively. Using an eight-channel high-voltage sequencer HVS448LC (Labsmith, Livermore, CA, USA), an electric field of 41.7 V/cm was applied for the first 15 min, followed by 125 V/cm until focusing was completed (3–5 min). Platinum electrodes (Nilaco, Tokyo, Japan) were used to apply an electric field.

Once IEF was completed, fluorescent images of focused bands were captured by scanning the entire microchannel using an IX70 microscope (Olympus, Tokyo, Japan), equipped with a motorized XY stage (MS-2000, ASI, Eugene, OR, USA), an sCMOS camera (Zyla, Andor, Belfast, UK), a LED light source (X-Cite Fire, Excelitas Technologies, Mississauga, Canada), and Metamorph software (Molecular Devices, San Jose, CA, USA). Images were captured at 2560 × 2160 pixels with an exposure time of 100 ms and 4 × 4 binning, and later stitched using the Multi-Dimensional Acquisition function of Metamorph. Image post-processing was performed using ImageJ (NI Health, Bethesda, MD, USA). Background signals of all images were subtracted with a 50-pixel rolling ball radius to account for background variation. The p*I* points of ZFP* and the ZFP*–DNA complex were measured based on pH gradients estimated by locations of focused p*I* markers. Noisy ZFP*–DNA fluorescence signals were smoothed by the Savitzky-Golay algorithm. Peak locations were found using a nonlinear Gaussian-peak-fitting algorithm in OriginPro 2019 software (OriginLab, Northampton, MA, USA).

2.6 Glass-Chip Preparation and On-Chip Discontinuous Polyacrylamide Gel Fabrication

Double-T junction glass microfluidic chips (Fig. 2a) were fabricated via isotropic wet etching (nominal width of 50 µm and depth of 20 µm) and thermal bonding by Perkin Elmer (Hopkinton, MA, USA). The inner microchannel surface was coated with a silane monolayer to facilitate covalent bonding of polyacrylamide gel (PAG) in the same manner as for the µIEF chip (Sect. 2.5).

Crosslinked PAG with discontinuous pore sizes was employed in this work to improve separation resolution (SR) between the ZFP*–DNA complex and protein internal standard (IS) to achieve rapid separation and sensitive peak detection (Fig. 2b). The PAG precursor solution consists of acrylamide/bis-acrylamide solution (29:1) of appropriate monomer concentrations (3 and 16%T), 0.2% (w/v) VA-086 photoinitiator, 1 × TG buffer (pH 8.6), and 0.1 mM $ZnCl_2$. The PAG precursor solution was vigorously

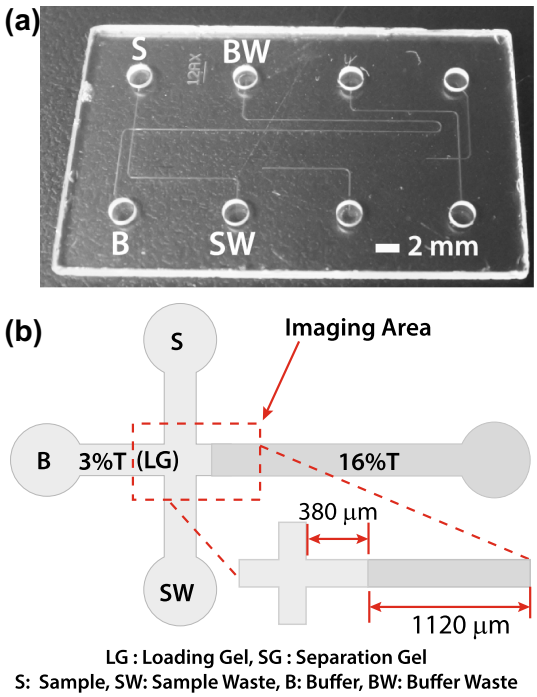

Fig. 2 Microfluidic chip and photopatterned polyacrylamide gel (PAG). **a** Photograph of the double-T junction glass microfluidic chip. **b** The microchannels house a discontinuous PAG consisting of 3%T loading gel (LG) and 16%T separation gel (SG). The LG-SG discontinuous interface was formed ~ 340 µm downstream from the junction. The full-field imaging area for the MEMRA is shown as a red dotted box

sonicated and degassed for 5 min before polymerization to ensure bubble-free PAG in the microchannels. Separation gel (SG) was fabricated by first loading concentrated precursor solution (16%T) into the microchannels by capillary action. Excess SG precursor solution was removed from the four wells (S, SW, B, and BW, Fig. 2a), and a drop of high-viscosity HEC solution (8% w/v) was applied to each well to prevent precursor evaporation. The chip was allowed to equilibrate for 5 min. The separation region of the microchannel (Fig. 2b) was exposed through the UV LED light source and 4 × objective lens (UPlanSAPO, Olympus) in the IX70 microscope at 12.5 mW/cm^2 for 90 s. UV intensity was measured using a digital UV meter UV-340A (Lutron Electronics, Coopersburg, PA, USA). Unpolymerized SG precursor solution was then replaced with loading-gel (LG) precursor solution (3%T) applying suction with caution to avoid introducing bubbles. LG precursor solution was then exposed to flood UV illumination of 5.0 W/cm^2 for 10 min using our custom-made UV exposure system. Finally, a glass microfluidic chip with photopatterned discontinuous gel was stored in 1 × TG + 0.1 mM $ZnCl_2$ buffer until usage.

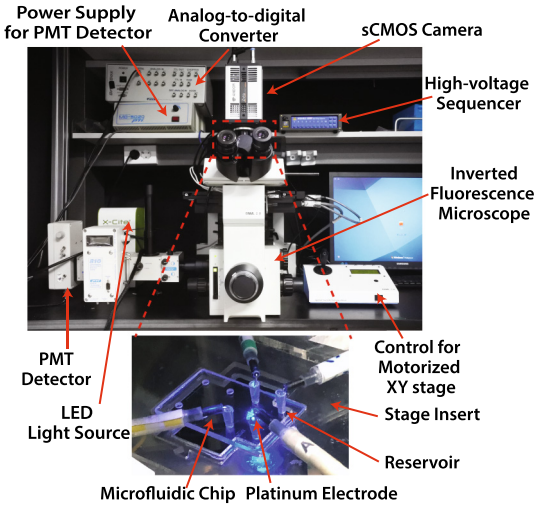

Fig. 3 Experimental setup for MEMRA. An inverted epi-fluorescence microscope, equipped with an sCMOS camera, LED light source, motorized stage, and PMT detection system was used for the assay. An 8-channel high-voltage sequencer was used for running the two-step electrophoresis assay by applying voltage programs to a four-terminal microfluidic chip (Fig. 2) through platinum electrodes

2.7 Operation of MEMRA Based on Full-Field Fluorescence Imaging

For quantitative MEMRA, full-field fluorescence imaging was performed using a 10 × objective lens UPLanFL (Olympus) and filter sets optimized for AF488 (39002AT, Chroma Technology, Bellows Falls, VT, USA) and Cy5 (Cy5-4040C-000, Semrock, Rochester, NY, USA) with the same IX70 microscope (Fig. 3). The image capture conditions were the same as for the p*I* measurement (Sect. 2.5). Peak area (area under the curve or AUC) was characterized similarly using OriginPro 2019.

The binding reaction between ZFP* and dsDNA oligonucleotides was performed in a 0.5 ml microcentrifuge tube using 20 µL of a solution containing the following constituents: 2.0 µM ZFP*, 10 nM BSA*, 20 nM unlabeled BSA, 1 mM DTT, 0.05% NP40, 1 × TG buffer, 0.1 mM $ZnCl_2$, and dsDNA in a concentration range of 10–500 nM. Cy-labeled dsDNA was used for assay-confirmation experiments, and unlabeled dsDNA for quantification experiments. The BSA* was used as a fluorescent internal standard for peak identification and accurate quantification by normalizing injection variability. DTT was added to reduce the disulfide bond of Cys residues in the ZFP. Unlabeled BSA was included to minimize the reduction effect of DTT on BSA*, because overall fluorescence signals were weak without the competing BSA. The role of $ZnCl_2$ was to provide zinc ions for ZFP coordination and to stabilize the folded protein structure [61]. The reaction mixture was incubated at 22 °C for 2 h (See Sect. 3.2.1).

The microfluidic chip was mounted in a custom-built polymethyl methacrylate (PMMA) chip holder that was inserted into the motorized stage, as seen in Fig. 3. Reservoirs (cut 200 µL pipette tips) were fitted tightly on each well. First, 10 µL of the incubated sample was loaded into the sample reservoir (S in Fig. 2). The other reservoirs (SW, B, and BW) were then filled with 20 µL of 1 × TG + 0.1 mM $ZnCl_2$ buffer. The high-voltage sequencer was used for applying electric fields and monitoring voltages and currents on each well. The same platinum electrodes were used to apply the electric field. The sample was electrophoretically injected into LG by applying 450 V to the SW reservoir and 100 V to other reservoirs for approximately 5 min (Fig. 4). The electric field was 122 V/cm in the loading channel, that is, from S to SW. The separation process was initiated by applying 1250 V in BW, 700 V in SW, 500 V in S and 200 V in BW reservoirs. The electric field was 175 V/cm in the separation channel, that is, from the cross-junction to BW. This electric field injected a sample plug into the separation microchannel, continuing to migrate toward BW. The sample plug was "stacked" (i.e., compacted) at the 3–16%T discontinuous PAG interface and separated in high resolution while migrating. Without a dsDNA present, positively charged ZFP would not be loaded from the S reservoir which is under a negative voltage, and excluded from the other species to be separated (Fig. 4a). With dsDNA, the polarity of ZFP-DNA will be reversed to negative, thereby allowing adequate loading and separation (Fig. 4b).

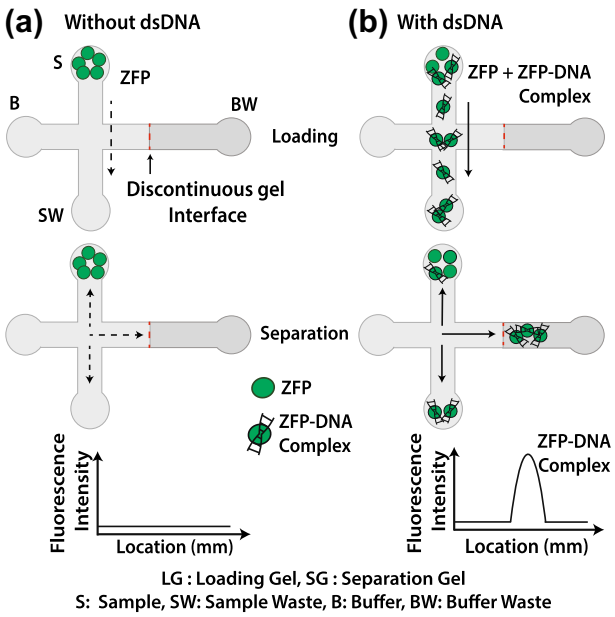

Fig. 4 MEMRA concept. **a** Positively charged ZFP remains in the S reservoir under loading and separation voltage programs in the absence of dsDNA. **b** With dsDNA, unbound ZFP remains in the S reservoir, but the ZFP–DNA complex migrates into the loading channel between S and SW under a loading voltage program. Next, the ZFP–DNA complex is pinch-injected as a molecular plug and is resolved in the separation channel (from the junction to BW) under a separation voltage program

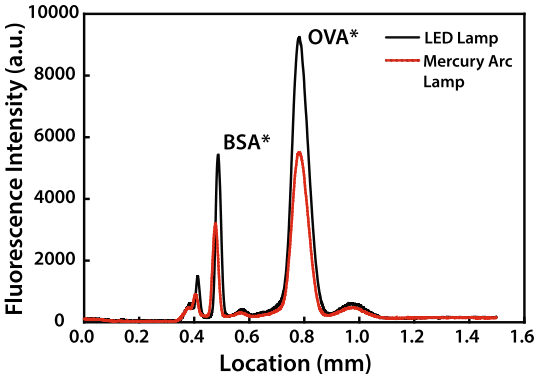

Fig. 5 Performance comparison of microscope fluorescence light sources. Fluorescence-labeled test proteins OVA* (200 nM) and BSA* (100 nM) were loaded and separated. The signal-to-noise ratios of fluorescence intensity obtained using the LED light source were ~ 2 × higher than those obtained using the mercury arc lamp

2.8 Single-Point Detection Based on a Photomultiplier Detector

Single-point detection was conducted using a photomultiplier tube (PMT) detector system (Photon Technology International, Birmingham, NJ, USA), consisting of a photo counter (model 810), microscope photometer (D-104), focusing eyepiece (CWHK 10X/18L, Olympus), and power supply (MD-5020). The photometer was mounted on the IX70 microscope (Fig. 3). A 40 × objective lens (LCPlanF1, Olympus) was focused on a defined detection point in the separation channel (~ 150 µm downstream from the discontinuous interface). Signals from the PMT detector were collected using an A/D converter (MUT BryteBox) and data-collection software (Felix32). Electropherograms (PMT signal vs. time) were generated by the software and imported to OriginPro 2019 for peak analysis. The same MEMRA condition (Sect. 2.7) was used for single-point detection, but in lower analyte concentrations of 100–1000 pM. The concentration of the internal-standard BSA* was also reduced to 2 nM to minimize peak overlap.

3 Results and Discussion

3.1 Development of the MEMRA

3.1.1 Selection of Light Source

Before working on the MEMRA, we sought to evaluate two fluorescence microscope light sources, a wide-band LED light source (X-Cite Fire) and a 100-W mercury arc lamp (U-ULH, Olympus) in terms of signal-to-noise ratio (SNR) using two AF488-labeled proteins, BSA* and OVA*. For this purpose, OVA* (200 nM) and BSA* (100 nM) were mixed off-chip, electrophoretically injected, and separated in the microfluidic chip with the 3–16% discontinuous PAG using the same MEMRA procedure (Sect. 2.7). Fluorescence intensities of the migrating bands were evaluated at the same migration distances from the cross junction (Fig. 2). The fluorescence intensity obtained using the LED light source gave rise to a ~ 2 × higher SNR than that of the mercury arc lamp, implying that a lower limit of detection could be achieved with the former (Fig. 5). Consequently, the LED light source was selected for further experiments. In addition to inducing higher intensity peaks, other benefits of the LED light source include more uniform brightness across captured images, less intensity variation over time (our experiments indicated × 1.5- × 4 less variability of injected BSA* bands), instant on and off operation (not feasible with a high-latency mechanical shutter), preheating circumvention, and a longer lifetime. Another useful advantage is that LED brightness can be readily adjusted by controlling the current without the need for neutral density filters.

3.1.2 Purification of ZFP–MBP Fusion Protein

Initially, we conducted a standard EMSA using ZFP fused with maltose-binding protein (MBP), an N-terminal purification tag (Sect. 2.3). After observing several persistent interfering bands during separation, we conducted SDS-PAGE on the ZFP sample and noted multiple bands, corresponding to the sizes of ZFP–MBP (62 kDa), MBP (42.5 kDa), and ZFP (19.5 kDa). It was speculated that autocleavage during the purification process possibly caused the multi-band problem. Thus, the fusion protein was cleaved by Factor Xa protease and purified to remove interfering MBP and ZFP–MBP. First, we employed affinity chromatography with amylose resin for the purification, but a faint SEB–MBP band was still present during separation. Thus, we resorted to a size-exclusion chromatography (FPLC) to completely remove all forms of MBP. After size-exclusion chromatography, the interfering bands arising from MBP and ZFP–MBP disappeared.

3.1.3 Selection of Internal Standard

An internal standard (IS), such as fluorescein, fluorescence-conjugated proteins or nucleic acids, is commonly used in quantitative microfluidic electrophoresis to account for chip-to-chip and run-to-run assay variations [62, 63]. We examined both BSA* and OVA* as an IS for peak-height normalization for ZFP* and the ZFP*–DNA complex. After several injections ($n = 5$), we found that both proteins have a similar injection variation (3.8–4.5% RSD in fluorescence intensity). However, having a higher molecular mass, BSA* (66.5 kDa) migrated slower than OVA* (42.7 kDa), and the OVA* band moved slower than the ZFP*–DNA complex. Therefore, the separation distance was higher for the BSA* IS, which is vital for high-resolution separation. We observed a few slower BSA bands, possibly originating from multimerization [64], but they did not interfere with the ZFP*–DNA complex band which migrated much faster. Therefore, BSA* was selected as our IS. After testing 25, 50, 100, and 200 nM BSA* for full-field imaging (Sect. 2.7), 25 nM was chosen for obtaining better SR as higher concentrations tended to increase peak width and reduced the SR. For PMT detection (Sect. 2.8) of lower DNA concentrations (100–1000 pM), 2 nM BSA* was used.

3.1.4 p*I* Measurement

Being an alkaline protein (theoretical p$I = 9.057$, calculated in Prot-p*I* [65]), ZFP is a challenging protein to analyze using the conventional EMSA format where target analyte, affinity probe, and analyte–probe complex migrate in the same direction in a electrophoresis buffer that has a pH higher than all their p*I* values (i.e., molecules are negatively charged, see Sect. 3.1.5 for further details). We observed significant smearing of the ZFP*–DNA bands during focusing, which could be attributed to DNA–carrier ampholyte interaction [66]. Precipitation was not alleviated even at 2.5% (w/v) CHAPS. After a few attempts, we opted for 5% CHAPS for minimizing precipitation. At higher CHAP concentrations, it was not easy to complete focusing. The p*I* points of ZFP* and ZFP*–DNA complex were determined to support the mobility-reversal concept and to select an appropriate electrophoretic buffer for the MEMRA. Several μIEF runs ($n = 7$) revealed that the estimated p*I* of the ZFP* is ~ 9.30 (Fig. 6a), while the ZFP*–DNA complex has a p*I* of ~ 5.33 (Fig. 6b).

3.1.5 Selection of Electrophoresis Buffer

Optimizing the pH of the electrophoresis buffer relative to analyte p*I*s is crucial for ensuring adequate injection and separation of all desired analytes. Hence, we evaluated three different buffer systems for our EMSA. We initially used 0.5 × TBE (Tris–borate EDTA) + 0.1 mM $ZnCl_2$ buffer (pH ~ 8.3) as a run buffer for EMSA development as TBE is a common electrophoresis buffer for nucleic acids. In this TBE buffer, ZFP*, ZFP*–DNA complex, and IS were all loaded and separated in the same direction,

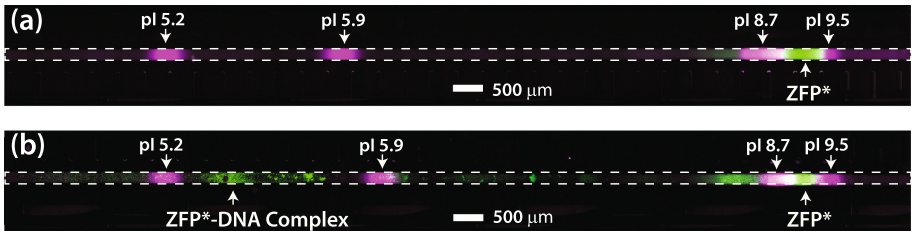

Fig. 6 Composite fluorescence images of ZFP*, the ZFP*–DNA complex, and standard p*I* markers (5.2, 5.9, 8.7, 9.5) focused by microfluidic isoelectric focusing (μIEF). **a** The p*I* of the control (2 μM ZFP*) was estimated to be 9.30 ± 0.07. **b** Upon binding with dsDNA (2.5 μM), the ZFP* forms a complex with a reduced p*I* of 5.33 ± 0.10. The IEF separation medium contains 6.25% (v/v) carrier ampholyte, 7.2% HEC (w/v), and 5% (w/v) CHAPS. An electric field of 41.7 V/cm was applied for the first 15 min followed by 125 V/cm for the remaining focusing time (3–5 min)

but multiple interfering ZFP* and ZFP*–DNA complex bands were observed. After we optimized MBP cleavage and chromatographic purification, the interfering bands disappeared. However, surprisingly, the ZFP* band also vanished from loading while the ZFP*–DNA complex band was adequately loaded and separated. Therefore, we found that a theoretical ZFP p*I* was 9.057. We also experimentally confirmed the alkalinity of ZFP using μIEF (Sect. 3.1.4). It was speculated that in the initial experiments the ZFP* isoforms with lower p*I*s were loaded and separated before optimizing the ZFP expression, cleavage, and purification processes, because p*I*s of ZFP* lower than the TBE buffer pH (p*I* = ~6.4 and ~8.1) were observed in the under-optimized ZFP* samples.

Thus, being unable to obtain ZFP* bands, we resorted to CAPS buffer, often used in alkaline electrophoresis [16]. CAPS buffer has a usable buffering range of pH 9.5–11.5 [67]. CAPS titrated to pH 10.75 was used as running buffer. As pH 10.75 was larger than the p*I*s of ZFP* and the ZFP*–DNA complex, both analytes were loaded into our microfluidic chip, seemingly suitable for EMSA. However, we faced two major obstacles. First, all species, including ZFP*, the ZFP*–DNA complex, and IS BSA*, especially ZFP*, smeared in the loading section of the chip at this pH. This unwanted interaction did not improve even after coating the inner channel surface with 5%T linear acrylamide (polymerized with UV illumination of 11 mW/cm^2 for 20 min) [68]. Smearing led to a considerable amount of protein being lost during loading. Interestingly, Cy5-labeled DNA did not show nonspecific interactions, indicating that ZFP* was the primary cause of smearing. A possible reason for the nonspecific adsorption could be acrylamide interactions with proteins at alkaline pH [50]. Second, all bands migrated considerably slower than in the TBE buffer and were dispersed rapidly after passing the LG–SG interface. Therefore, the separation of ZFP*, the ZFP*–DNA complex, and IS* was challenging. Protein smearing and band dispersion were unpredictable, rendering quantitative analysis challenging if not impossible. We also noted that these problems were exacerbated when the CAPS buffer pH increased to 11. Moreover, PAG readily degraded (forming bubbles) at high pHs (failed after 10–13 injections vs. more than 30 injections in the TBE buffer). Several remedies were attempted to improve loading and separation in the CAPS buffer including: (1) addition of the nonionic detergent Tween 20 (0.05–0.5% v/v) to PAG precursor solutions and to the ZFP*–DNA binding reaction to reduce nonspecific adsorption; and (2) extending the polymerization time to prevent possible nonspecific interactions between unpolymerized acrylamide and proteins [50]. Both remedies failed to improve the nonspecific adsorption and analyte dispersion. Therefore, we concluded that the strongly alkaline CAPS buffer was not suitable either.

Therefore, instead of further pursuing the conventional EMSA approach, we devised the novel concept of MEMRA to reverse ZFP* mobility upon binding with dsDNA in a mildly alkaline buffer (1 × TG at pH 8.6). In the conventional EMSA format, the amounts of both unbound probe and complex should be measured to estimate the binding affinity or characterize interaction kinetics [1, 15, 23]. However, for direct (i.e., not competitive) quantitation of DNA, the unbound ZFP* band does not have to co-migrate with the ZFP*–DNA band. DNA concentration can be measured using a fluorescent ZFP*–DNA complex and a co-migrating IS* (for normalization) [7, 14, 18]. ZFP* should be positively charged in 1 × TG buffer (pH 8.6), because its p*I* value (9.3) is higher. In contrast, the ZFP*–DNA complex (p*I* = 5.33) should be negatively charged under the same conditions. The TG buffer was chosen, because it is a common electrophoresis buffer for EMSA or HEAA for proteins [7, 18, 69, 70]. Additionally, the measured electrophoresis current was lower than in the TBE buffer system, reducing detrimental heat generation.

To materialize our MEMRA concept in TG buffer, we conducted multiple negative-control experiments without target dsDNA. Figure 7a illustrates a typical separation montage and resulting electropherogram for ZFP* and IS* (i.e., BSA*). As expected from their p*I*s, the application of 1 × TG buffer resulted in positively charged ZFP*, which was prevented from leaving the S reservoir. Only the IS* was injected (slower, smaller peaks for higher-molecular-mass BSA multimers were also observed). Next, we ran positive-control experiments with ZFP* incubated with 100 nM Cy5-labeled *seb* dsDNA* oligonucleotides to identify the ZFP*–DNA* complex band and confirm mobility reversal. Only the ZFP*–DNA* complex and IS* were injected and fully separated, as shown in Fig. 7b. Owing to the discontinuous PAG, an initially dispersed sample plug condensed after passing the LG–SG interface. Therefore, rapid, high-resolution separation was achieved; the complex peak was fully resolved (SR ≥ 2.0) from the IS* in just 15 s when the separation electric field was 175 V/cm. Complete exclusion of unbound ZFP* from the separating species prevented zone interference with the ZFP*–DNA* complex that occurred in the CAPS buffers and afforded rapid, high-resolution separation. The rapid separation would enable high-throughput dsDNA detection. The separation distance, that is, the migration distance of a leading peak upon separation completion, was also remarkably short: ~160 μm from the discontinuous interface. Such a short separation distance would allow for a small device footprint. As seen on the electropherograms for both negative and positive control experiments, there were no observable nonspecific interactions or rapid band dispersion in contrast to the electrophoresis results in the CAPS buffer. A key advantage of our DNA assay is that DNA denaturation and subsequent renaturation

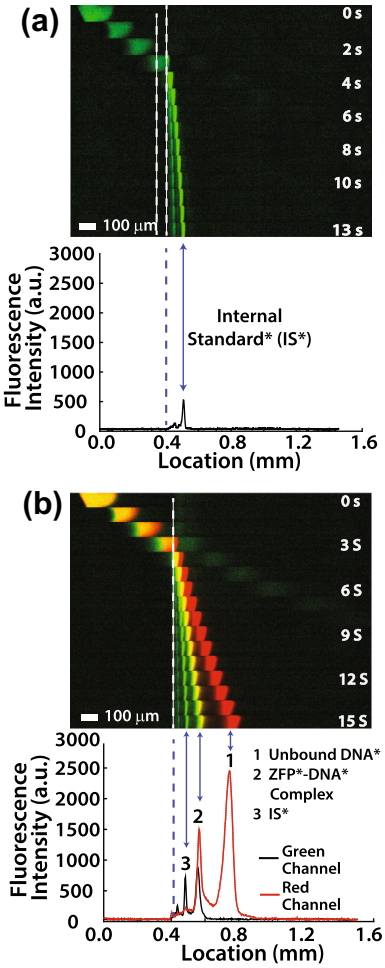

Fig. 7 MEMRA confirmation. **a** Separation montage and electropherogram for the negative control (no DNA present). The electropherogram was obtained 13 s after separation commenced. ZFP* was completely excluded from loading, because its p*I* (9.3) was higher than the buffer pH (8.6). **b** Multi-color separation montage and electropherogram for the positive control (100 nM Cy-5 labeled *seb*-gene dsDNA* oligonucleotides incubated with ZFP*). The electropherogram was obtained 15 s after separation commenced. The ZFP*–DNA* complex and IS* were properly loaded and fully separated (separation resolution ≥ 2.0). Assay conditions: sample = 2.0 μM ZFP* and 10 nM IS* (BSA*) in 1 mM DTT + 0.05% NP 40 + 0.1 mM $ZnCl_2$ + 1 × TG buffer, electrophoresis buffer = 1 × TG + 0.1 mM $ZnCl_2$, and separation electric field = 175 V/cm

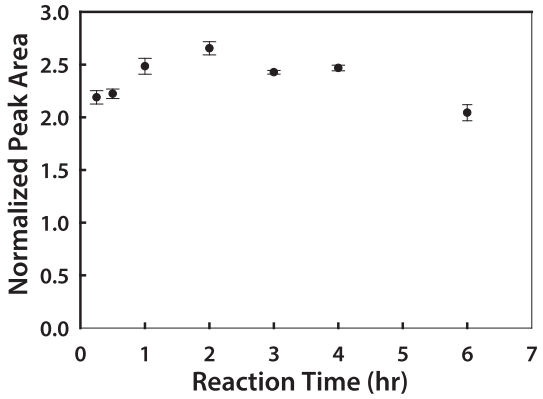

Fig. 8 Determination of binding reaction time for ZFP* and DNA. The reactants are 2 μM ZFP*, 1 μM unlabeled dsDNA in 1 mM DTT + 0.05% NP 40 + 0.1 mM $ZnCl_2$ + 1 × TG buffer. The electrophoresis conditions were the same as those in Fig. 7. Error bars indicate the standard deviations of triplicate experiments

processes were not required, in contrast to most ssDNA-hybridization-based DNA detection methods.

3.2 Characterization of Quantitative MEMRA Assay

3.2.1 Determination of Binding-Reaction Time

Having established the electrophoretic buffer, the binding-reaction time in the MEMRA for *unlabeled* dsDNA was experimentally optimized. The fluorescence intensity of separated ZFP*-DNA complexes was quantified at binding-reaction times increasing from 0.25 to 6 h for the same concentration of binding reactants. Figure 8 shows the normalized peak area of the ZFP*–DNA complex ($n = 3$) as a function of reaction time. As seen in the graph, a substantial amount of ZFP*–DNA complex (normalized peak area = 2.19) was formed after only 0.25 h. With a reaction of 2 h, we observed the maximized ZDP–DNA complex formation (2.69). After 2 h, the amount of ZFP*–DNA complex decreased somewhat, compared to the maximum. Furthermore, the signal for the ZFP*–DNA complex formed at 6 h was even smaller than that at 0.25 h. The reason for this reduction is not clear at present, but may result from a loss of binding activity due to prolonged exposure to room temperature. Thus, we selected 2 h as the optimal binding reaction time.

3.2.2 Qualitative dsDNA Analysis Using Full-Field Imaging

To assess its quantitation capability, the MEMRA was performed with known concentrations of unlabeled *seb* dsDNA oligonucleotides (10–500 nM). Figure 9a shows a separation result of the MEMRA for 20 nM dsDNA using full-field fluorescence imaging. The ZFP*–DNA complex was fully separated after 12 s at ~ 240 μm separation distance. The electrophoretic behavior of the ZFP*–DNA complex was similar to that of the ZFP*–DNA* complex (Cy5-conjugated dsDNA) shown in Fig. 7.

After confirming separation and detection of unlabeled dsDNA, quantitation performance was analyzed by constructing a dose–response curve. First, the fluorescence intensity (AUC) of the ZFP*–DNA complex of varying concentrations (0–500 nM), normalized by the AUC of each co-migrating IS* peak, was plotted (Fig. 9b). A

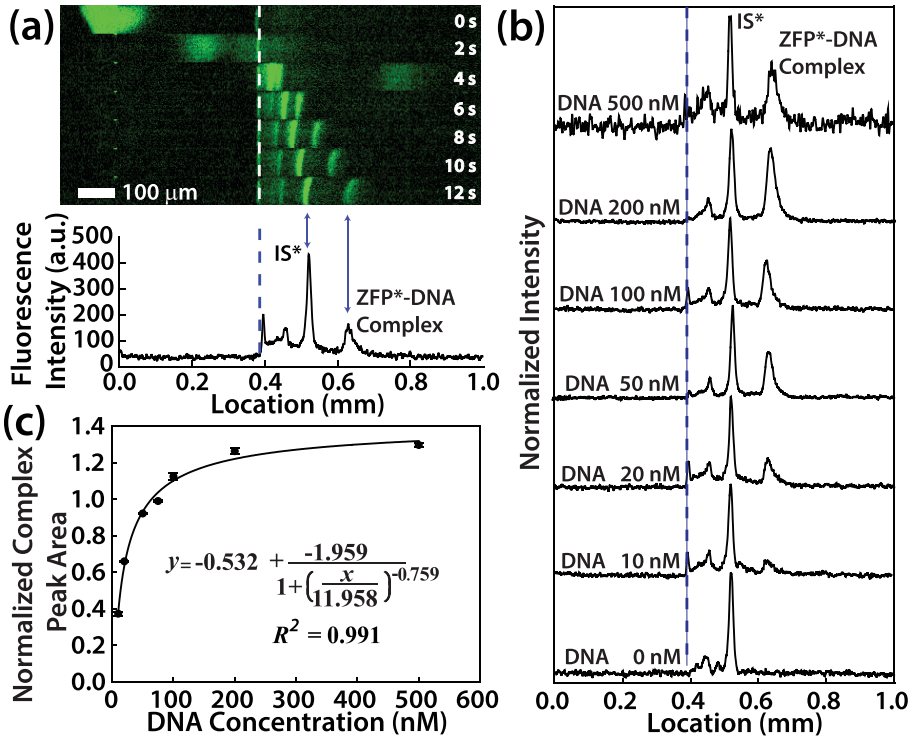

Fig. 9 MEMRA characterization based on full-field fluorescence imaging. **a** The optimized separation conditions (Sects. 3.1.5 and 3.2.1) enabled the detection of unlabeled 20 nM *seb* gene dsDNA oligonucleotides. The separation time was 12 s, and the separation distance was ~ 240 μm (from the discontinuous interface). The assay conditions are the same as those applied for Fig. 7. **b** Electropherograms of dsDNA at 10–500 nM concentration range. The area (AUC) of the ZFP*–DNA peak was normalized by each co-migrating IS* peak. As dsDNA concentration increased, the normalized complex-peak area increased as well. The noisy electropherogram for the 500 nM case is evidence of injection variability (lower amounts of sample were loaded compared to the other cases). **c** A sigmoidal dose–response curve ($R^2 = 0.991$) for dsDNA. Error bars refer to standard deviations of triplicate runs ($n = 3$). The limit of detection was 7.8 nM based on a linear region of lower concentrations (10 – 125 nM) and the background signal (0 nM dsDNA)

dose–response curve was constructed by curve fitting the normalized intensities with a 4-parameter logistic equation ($R^2 = 0.991$) using OriginPro software (Fig. 9c). The limit of detection (LOD) was determined to be 7.8 nM using a linear calibration curve obtained for a lower linear region of the dose–response curve (10–125 nM) and background signal at 0 nM dsDNA (Fig. 9b).

3.2.3 Quantitative dsDNA Analysis Using Sensitive Single-Point Detection

To evaluate the quantitation limit of the MEMRA, we conducted single-point detection using a photomultiplier-tube (PMT) detection system and the same LED light source. Because of the high sensitivity of the PMT system, lower analyte concentrations of 100–1000 pM were measured. At this assay condition, the IS* concentration was also lowered (2 nM) to maintain separation resolution adequate as larger IS* peak widths resulted from higher concentrations. The ZFP* concentration was also halved to 1 μM, which was still excessive compared to the amount of target dsDNA (1:1000–1:10,000). As expected, unbound ZFP* was not loaded and did not interfere with the MEMRA. The position of the pinhole aperture for PMT detection was set ~ 150 μm downstream from the discontinuous interface. The same MEMRA conditions as those described in Sect. 3.2.2 were used for single-point detection, except for the lower ZFP* and IS* concentrations.

Figure 10a shows the PMT electropherograms (normalized by IS*-peak height) for the positive control (100 pM dsDNA) and negative control (no dsDNA). The ZFP*–DNA complex and IS* peaks were baseline-separated (SR ≥ 1.5) at this single-point location. We noted an unidentified peak after the residual AF488 dye peak, which was not relevant to DNA concentration and did not hinder the MEMRA. A linear calibration curve was also constructed using normalized peak heights of varying dsDNA concentrations (Fig. 10b). An impressive LOD of ~ 50 pM was obtained using the calibration curve and background signal of the negative control data (Fig. 10a). Considering the smallest obtainable complex peak volume of 1.2×10^{-7} ml (measured using full-field imaging for the 10 nM DNA case, Fig. 9)

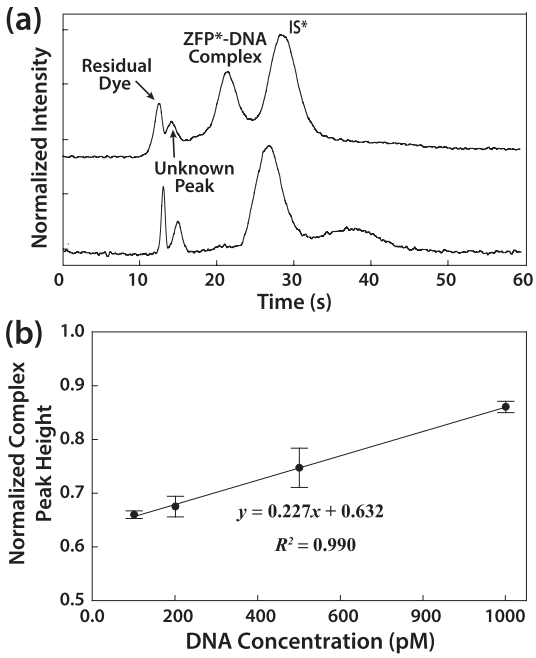

Fig. 10 Single-point detection for MEMRA. **a** Positive control (100 pM DNA) and negative control (no DNA) confirmed that our MEMRA can detect pM-range dsDNA without denaturation and renaturation. The pinhole location was ~150 µm downstream from the discontinuous interface. **b** A linear dose–response curve for dsDNA quantification for the 100–1000 pM concentration range ($R^2 = 0.990$). The LOD was ~ 50 pM. The MEMRA conditions were identical to those given in Fig. 7 except for the use of lower IS* (2 nM) and ZFP* concentrations (1 µM)

and the lowest detected concentration (100 pM), dsDNA of ~ 10^4 copies could be measured if material loss during loading was minimized; this can be achieved, for example, by reducing reservoir volumes, shortening the loading channel, and/or integrating transient isotachophoresis [71, 72]). At this quantitation level, the amount of *S. aureus* from food poisoning, 10^5–10^6 cells per ml of food [73, 74], could be rapidly detected without cell culture or nucleic-acid amplification if adequate sample collection and treatment methods were incorporated. *S. aureus* could also be detected from pus or infected peritoneal fluid samples directly as the amount reaches 10^8 cells/ml [75, 76]. Currently, we are optimizing the single-point detection by adjusting binding reaction and electrophoresis conditions to lower the LOD.

Taken together, we have demonstrated the feasibility of ZFP-based HEAA by adopting the novel concept of detection-probe mobility reversal upon binding with target DNA. Time-consuming and tedious DNA denaturation and renaturation were circumvented by employing ZFP, a specific dsDNA-binding protein motif. Incorporating a photopatterned discontinuous PAG system, extremely effective separation (separation time as fast as 12 s and separation distance as short as 160 µm) was achieved, which is anticipated to enable high-throughput dsDNA detection with a small device footprint in the future. Finally, an LOD of ~ 50 pM was achieved by incorporating a sensitive PMT detection, which may render amplification-free detection of bacteria viable in some limited cases. Table 1 qualitatively compares the MEMRA with previous hybridization-based microfluidic DNA assays [77].

4 Conclusion

Rapid, sensitive, sequence-specific DNA detection has always been highly desirable as it is necessary for a myriad of applications in biology and medicine, including microbiology, forensics, genotyping, and genetic and infectious disease diagnoses. DNA analysis in a microfluidic format promises low sample and reagent consumption, automated

Table 1 Qualitative comparison of the MEMRA with hybridization-based microfluidic DNA assays [77]

	MEMRA	Hybridization-based microfluidic DNA assays
Pros	No denaturation and renaturation required	Well established method
	No wash required	Easier design of detection probe (ssDNA)
	No probe immobilization required	Cheaper and simpler production of detection probe (ssDNA)
	Simpler chip design and fabrication (cross-junction chip)	
	Faster assay	
Cons	Relatively new method	Denaturation and renaturation (hybridization) required
	More complex and time-consuming design of detection probe (ZFP)	Wash required (except molecular beacons)
	More expensive and time-consuming production of detection probe (ZFP)	Probe immobilization required (heterogenous assay types)
		More complex chip design and fabrication (multistep assay)
		Slower assay
		Strongly negatively charged probe (ssDNA) may cause assay complications (nonspecific binding with interfering species)

workflow, expedited results, and a small device form factor. However, the majority of conventional microfluidic DNA analyses depend on time-consuming and tedious single-stranded DNA (ssDNA) hybridization approaches requiring denaturation and renaturation, detracting from the assay performance.

As an elegant solution to this problem, we propose for the first time a microfluidic electrophoretic homogeneous affinity assay (HEAA) based on a novel zinc-finger protein (ZFP) detection probe. ZFP binds directly to a specific sequence of double-stranded DNA (dsDNA), mitigating the critical limitation of ssDNA hybridization approaches. Herein, we demonstrated rapid, sensitive, and specific detection of the 18-bp target dsDNA of the *seb* (*Staphylococcus* enterotoxin B) gene oligonucleotides, employing HEAA and an engineered ZFP. The key to success was to employ the novel concept of mobility reversal in our microfluidic electrophoretic mobility reversal assay (MEMRA), a type of electrophoretic mobility shift assay (EMSA), using a rationally selected and experimentally evaluated electrophoresis buffer. The reversed migration of the ZFP detection probe upon binding with target dsDNA in the mildly alkaline tris–glycine buffer, completely excluded unassociated ZFP from loading, and addressed the drawbacks of protein smearing and band dispersion, observed in the strongly alkaline CAPS buffer. The MEMRA also exhibited outstanding assay performance, including rapid separations (12–15 s) and short separation distances (160–240 μm) with the aid of on-chip photopatterned 3–16% discontinuous polyacrylamide gel (PAG).

The MEMRA process was complete within ~ 3 min, excluding the ZFP-dsDNA-binding reaction. A binding reaction time of 2 h was employed for maximum association but the reaction time can be reduced to 15 min with an acceptable loss of signal intensity (17.5%, calculated from Fig. 8). Therefore, the overall assay time, from target-probe incubation to detection, could be less than 20 min. The two-orders-of-magnitude dynamic range of 10–500 nM and an LOD of 7 nM were achieved using fluorescence full-field imaging based on an sCMOS camera and a broadband LED source. An outstanding LOD of 50 pM was obtained using a PMT detection system without exhaustive assay optimization. At this level of sensitivity and the estimated number of detected dsDNA molecules during electrophoretic separation, dsDNA oligonucleotides from food or biological samples, such as spoiled foodstuff, pus, or infected peritoneal fluids, could be directly analyzed with suitable sample collection and preparation. The extremely short separation distance, afforded by the discontinuous PAG, would allow for a small device footprint and straightforward device parallelization.

We expect that our ZFP-based MEMRA will be widely used for rapid, quantitative, specific gene analysis in the near future. We are currently optimizing the MEMRA to achieve enhanced LOD and throughput, detection of the *seb* gene from extracted *S. aureus* genomic DNA, and to expand assay applicability toward detection of Shiga toxin from *E. coli*.

Acknowledgements This work was supported by Basic Science Research Programs through the National Research Foundation of Korea (NRF) funded by the Korean government (MSIT) (2019R1F1A1043885). This work was also supported by the Korea Institute of Energy Technology Evaluation and Planning (KETEP) and the Ministry of Trade, Industry & Energy (MOTIE) of the Republic of Korea (No. 20194010201750).

Declarations

Conflict of interest The authors declare no competing financial interests.

References

1. Pan, Y., Karns, K., Herr, A.E.: Microfluidic electrophoretic mobility shift assays for quantitative biochemical analysis. Electrophoresis **35**, 2078–2090 (2014)
2. Hou, C., Herr, A.E.: Clinically relevant advances in on-chip affinity-based electrophoresis and electrochromatography. Electrophoresis **29**, 3306–3319 (2008)
3. Schmalzing, D., Nashabeh, W.: Capillary electrophoresis based immunoassays: a critical review. Electrophoresis **18**, 2184–2193 (1997)
4. He, X., Ding, Y., Li, D., Lin, B.: Recent advances in the study of biomolecular interactions by capillary electrophoresis. Electrophoresis **25**, 697–711 (2004)
5. Schou, C., Heegaard, N.H.: Recent applications of affinity interactions in capillary electrophoresis. Electrophoresis **27**, 44–59 (2006)
6. Dey, B., Thukral, S., Krishnan, S., Chakrobarty, M., Gupta, S., Manghani, C., Rani, V.: DNA–protein interactions: methods for detection and analysis. Mol. Cell. Biochem. **365**, 279–299 (2012)
7. Hou, C., Herr, A.E.: Ultrashort separation length homogeneous electrophoretic immunoassays using on-chip discontinuous polyacrylamide gels. Anal. Chem. **82**, 3343–3351 (2010)
8. Cheng, S.B., Skinner, C.D., Taylor, J., Attiya, S., Lee, W.E., Picelli, G., Harrison, D.J.: Development of a multichannel microfluidic analysis system employing affinity capillary electrophoresis for immunoassay. Anal. Chem. **73**, 1472–1479 (2001)
9. Bromberg, A., Mathies, R.A.: Multichannel homogeneous immunoassay for detection of 2, 4, 6-trinitrotoluene (TNT) using a microfabricated capillary array electrophoresis chip. Electrophoresis **25**, 1895–1900 (2004)
10. Kuswandi, B., Nuriman, H.J., Verboom, W.: Optical sensing systems for microfluidic devices: a review. Anal. Chim. Acta **601**, 141–155 (2007)
11. Schultz, N.M., Kennedy, R.T.: Rapid immunoassays using capillary electrophoresis with fluorescence detection. Anal. Chem. **65**, 3161–3165 (1993)
12. Shimura, K., Karger, B.L.: Affinity probe capillary electrophoresis: analysis of recombinant human growth hormone with a fluorescent labeled antibody fragment. Anal. Chem. **66**, 9–15 (1994)
13. Koutny, L.B., Schmalzing, D., Taylor, T.A., Fuchs, M.: Microchip electrophoretic immunoassay for serum cortisol. Anal. Chem. **68**, 18–22 (1996)

14. Chiem, N., Harrison, D.J.: Microchip-based capillary electrophoresis for immunoassays: analysis of monoclonal antibodies and theophylline. Anal. Chem. **69**, 373–378 (1997)
15. Chiem, N.H., Harrison, D.J.: Monoclonal antibody binding affinity determined by microchip-based capillary electrophoresis. Electrophoresis **19**, 3040–3044 (1998)
16. Karns, K., Herr, A.E.: Human tear protein analysis enabled by an alkaline microfluidic homogeneous immunoassay. Anal. Chem. **83**, 8115–8122 (2011)
17. Schmalzing, D., Koutny, L.B., Taylor, T.A., Nashabeh, W., Fuchs, M.: Immunoassay for thyroxine (T4) in serum using capillary electrophoresis and micromachined devices. J. Chromatogr. B Biomed. Sci. Appl. **697**, 175–180 (1997)
18. Herr, A.E., Throckmorton, D.J., Davenport, A.A., Singh, A.K.: On-chip native gel electrophoresis-based immunoassays for tetanus antibody and toxin. Anal. Chem. **77**, 585–590 (2005)
19. Clark, J., Shevchuk, T., Swiderski, P.M., Dabur, R., Crocitto, L.E., Buryanov, Y.I., Smith, S.S.: Mobility-shift analysis with microfluidics chips. Biotechniques **35**, 548–555 (2003)
20. Xian, J., Harrington, M.G., Davidson, E.H.: DNA-protein binding assays from a single sea urchin egg: a high-sensitivity capillary electrophoresis method. Proc. Natl. Acad. Sci. USA **93**, 86–90 (1996)
21. Foulds, G.J., Etzkorn, F.A.: A capillary electrophoresis mobility shift assay for protein—DNA binding affinities free in solution. Nucleic Acids Res. **26**, 4304–4305 (1998)
22. Hu, J., Easley, C.J.: A simple and rapid approach for measurement of dissociation constants of DNA aptamers against proteins and small molecules via automated microchip electrophoresis. Analyst **136**, 3461–3468 (2011)
23. Huber, D.E., Markel, M.L., Pennathur, S., Patel, K.D.: Oligonucleotide hybridization and free-solution electrokinetic separation in a nanofluidic device. Lab Chip **9**, 2933–2940 (2009)
24. Liu, P., Mathies, R.A.: Integrated microfluidic systems for high-performance genetic analysis. Trends Biotechnol. **27**, 572–581 (2009)
25. Gorgannezhad, L., Stratton, H., Nguyen, N.-T.: Microfluidic-based nucleic acid amplification systems in microbiology. Micromachines **10**, 408 (2019)
26. Bae, S., Son, K., Lee, D., Han, S., Choi, K., Kim, S.: Warfarin pharmacogenetics: single-nucleotide polymorphism detection using CMOS photosensor-based real-time PCR. Biochip J. **14**, 204–210 (2020)
27. Bruijns, B., Van Asten, A., Tiggelaar, R., Gardeniers, H.: Microfluidic devices for forensic DNA analysis: a review. Biosensors **6**, 41 (2016)
28. Hardenbol, P., Banér, J., Jain, M., Nilsson, M., Namsaraev, E.A., Karlin-Neumann, G.A., Fakhrai-Rad, H., Ronaghi, M., Willis, T.D., Landegren, U., Davis, R.W.: Multiplexed genotyping with sequence-tagged molecular inversion probes. Nat. Biotechnol. **21**, 673–678 (2003)
29. Chen, D., Shen, X., Xu, Y., Cai, B., Ding, C., Zhong, Y., Xu, Y., Zhou, C.: Next-generation sequencing-based preimplantation genetic testing for de novo NF1 mutations. Biochip J. **15**, 69–76 (2021)
30. Schena, M., Shalon, D., Davis, R.W., Brown, P.O.: Quantitative monitoring of gene expression patterns with a complementary DNA microarray. Science **270**, 467–470 (1995)
31. Lu, Y., Chen, S., Wei, L., Sun, L., Liu, H., Xu, Y.: A microfluidic-based SNP genotyping method for hereditary hearing-loss detection. Anal. Chem. **91**, 6111–6117 (2019)
32. Mothershed, E.A., Whitney, A.M.: Nucleic acid-based methods for the detection of bacterial pathogens: present and future considerations for the clinical laboratory. Clin. Chim. Acta **363**, 206–220 (2006)
33. Paillard, F., Hill, C.S.: Direct nucleic acid diagnostic tests for bacterial infectious diseases: streptococcal pharyngitis, pulmonary tuberculosis, vaginitis, chlamydial and gonococcal infections. MLO Med. Lab. Obs. **36**, 10–15 (2004). (**quiz 16**)
34. Na, H., Kang, B.-H., Ku, J., Kim, Y., Jeong, K.-H.: On-chip paper electrophoresis for ultrafast screening of infectious diseases. Biochip J. **15**, 305–311 (2021)
35. Kim, J.H., Kang, M., Park, E., Chung, D.R., Kim, J., Hwang, E.S.: A simple and multiplex loop-mediated isothermal amplification (LAMP) assay for rapid detection of SARS-CoV. Biochip J. **13**, 341–351 (2019)
36. Burns, M.A., Johnson, B.N., Brahmasandra, S.N., Handique, K., Webster, J.R., Krishnan, M., Sammarco, T.S., Man, P.M., Jones, D., Heldsinger, D.: An integrated nanoliter DNA analysis device. Science **282**, 484–487 (1998)
37. Niemz, A., Ferguson, T.M., Boyle, D.S.: Point-of-care nucleic acid testing for infectious diseases. Trends Biotechnol. **29**, 240–250 (2011)
38. Vahedi, G., Kaler, K., Backhouse, C.J.: An integrated method for mutation detection using on-chip sample preparation, single-stranded conformation polymorphism, and heteroduplex analysis. Electrophoresis **25**, 2346–2356 (2004)
39. Kim, M.-S., Stybayeva, G., Lee, J.Y., Revzin, A., Segal, D.J.: A zinc finger protein array for the visual detection of specific DNA sequences for diagnostic applications. Nucleic Acids Res. **39**, gkq1214 (2010)
40. Ghosh, I., Stains, C.I., Ooi, A.T., Segal, D.J.: Direct detection of double-stranded DNA: molecular methods and applications for DNA diagnostics. Mol. Biosyst. **2**, 551–560 (2006)
41. Biet, E., Sun, J.S., Dutreix, M.: Conserved sequence preference in DNA binding among recombination proteins: an effect of ssDNA secondary structure. Nucleic Acids Res. **27**, 596–600 (1999)
42. Klug, A., Rhodes, D.: 'Zinc fingers': a novel protein motif for nucleic acid recognition. Trends Biochem. Sci. **12**, 464–469 (1987)
43. Segal, D.J., Barbas, C.F., III.: Custom DNA-binding proteins come of age: polydactyl zinc-finger proteins. Curr. Opin. Biotechnol. **12**, 632–637 (2001)
44. Beerli, R.R., Segal, D.J., Dreier, B., Barbas, C.F.: Toward controlling gene expression at will: specific regulation of the erbB-2/HER-2 promoter by using polydactyl zinc finger proteins constructed from modular building blocks. Proc. Natl. Acad. Sci. USA **95**, 14628–14633 (1998)
45. Liu, Q., Segal, D.J., Ghiara, J.B., Barbas, C.F.: Design of polydactyl zinc-finger proteins for unique addressing within complex genomes. Proc. Natl. Acad. Sci. USA **94**, 5525–5530 (1997)
46. Dreier, B., Beerli, R.R., Segal, D.J., Flippin, J.D., Barbas, C.F.: Development of zinc finger domains for recognition of the 5′-ANN-3′ family of DNA sequences and their use in the construction of artificial transcription factors. J. Biol. Chem. **276**, 29466–29478 (2001)
47. Segal, D.J., Dreier, B., Beerli, R.R., Barbas, C.F.: Toward controlling gene expression at will: selection and design of zinc finger domains recognizing each of the 5′-GNN-3′ DNA target sequences. Proc. Natl. Acad. Sci. USA **96**, 2758–2763 (1999)
48. Segal, D.J., Beerli, R.R., Blancafort, P., Dreier, B., Effertz, K., Huber, A., Koksch, B., Lund, C.V., Magnenat, L., Valente, D., Barbas, C.F., 3rd.: Evaluation of a modular strategy for the construction of novel polydactyl zinc finger DNA-binding proteins. Biochemistry **42**, 2137–2148 (2003)
49. Mangru, S.D., Harrison, D.J.: Chemiluminescence detection in integrated post-separation reactors for microchip-based capillary electrophoresis and affinity electrophoresis. Electrophoresis **19**, 2301–2307 (1998)

50. Geisthardt, D., Kruppa, J.: Polyacrylamide gel electrophoresis: reaction of acrylamide at alkaline pH with buffer components and proteins. Anal. Biochem. **160**, 184–191 (1987)
51. Kim, D., Karns, K., Tia, S.Q., He, M., Herr, A.E.: Electrostatic protein immobilization using charged polyacrylamide gels and cationic detergent microfluidic western blotting. Anal. Chem. **84**, 2533–2540 (2012)
52. Brahmasandra, S.N., Ugaz, V.M., Burke, D.T., Mastrangelo, C.H., Burns, M.A.: Electrophoresis in microfabricated devices using photopolymerized polyacrylamide gels and electrode-defined sample injection. Electrophoresis **22**, 300–311 (2001)
53. Neville, D.M.: Molecular weight determination of protein-dodecyl sulfate complexes by gel electrophoresis in a discontinuous buffer system. J. Biol. Chem. **246**, 6328–6334 (1971)
54. Chung, M., Kim, D., Herr, A.E.: Polymer sieving matrices in microanalytical electrophoresis. Analyst **139**, 5635–5654 (2014)
55. Koydemir, H.C., Külah, H., Özgen, C., Alp, A., Hasçelik, G.: MEMS biosensors for detection of methicillin resistant *Staphylococcus aureus*. Biosens. Bioelectron. **29**, 1–12 (2011)
56. Bhatia, A., Zahoor, S.: *Staphylococcus aureus* enterotoxins: a review. J. Clin. Diagn. Res. **3**, 188–197 (2007)
57. Gilligan, K., Shipley, M., Stiles, B., Hadfield, T., Ibrahim, M.S.: Identification of *Staphylococcus aureus* enterotoxins A and B genes by PCR-ELISA. Mol. Cell. Probes **14**, 71–78 (2000)
58. Yuan, H., Liu, Y., Jiang, X., Xu, S., Sui, G.: Microfluidic chip for rapid analysis of cerebrospinal fluid infected with *Staphylococcus aureus*. Anal. Methods **6**, 2015–2019 (2014)
59. Bhakta, M.S., Segal, D.J.: The generation of zinc finger proteins by modular assembly. In: Engineered zinc finger proteins, pp. 3–30. Springer (2010)
60. Ha, D.T., Ghosh, S., Ahn, C.H., Segal, D.J., Kim, M.-S.: Pathogen-specific DNA sensing with engineered zinc finger proteins immobilized on a polymer chip. Analyst **143**, 4009–4016 (2018)
61. Kluska, K., Adamczyk, J., Krężel, A.: Metal binding properties, stability and reactivity of zinc fingers. Coord. Chem. Rev. **367**, 18–64 (2018)
62. Duncombe, T.A., Herr, A.E.: Photopatterned free-standing polyacrylamide gels for microfluidic protein electrophoresis. Lab Chip **13**, 2115–2123 (2013)
63. Meagher, R.J., Hatch, A.V., Renzi, R.F., Singh, A.K.: An integrated microfluidic platform for sensitive and rapid detection of biological toxins. Lab Chip **8**, 2046–2053 (2008)
64. Bryan, J.: Molecular weights of protein multimers from polyacrylamide gel electrophoresis. Anal. Biochem. **78**, 513–519 (1977)
65. Prot pi Protein Tool. https://www.protpi.ch/Calculator/ProteinTool. Accessed 31 Aug 2021
66. Leimgruber, R.M., Malone, J.P., Radabaugh, M.R., LaPorte, M.L., Violand, B.N., Monahan, J.B.: Development of improved cell lysis, solubilization and imaging approaches for proteomic analyses. Proteomics **2**, 135–144 (2002)
67. Ferreira, C.M., Pinto, I.S., Soares, E.V., Soares, H.M.: (Un) suitability of the use of pH buffers in biological, biochemical and environmental studies and their interaction with metal ions—a review. RSC Adv. **5**, 30989–31003 (2015)
68. Hou, C., Herr, A.E.: Microfluidic integration of Western blotting is enabled by electrotransfer-assisted sodium dodecyl sulfate dilution. Analyst **138**, 158–163 (2013)
69. Herr, A.E., Hatch, A.V., Throckmorton, D.J., Tran, H.M., Brennan, J.S., Giannobile, W.V., Singh, A.K.: Microfluidic immunoassays as rapid saliva-based clinical diagnostics. Proc. Natl. Acad. Sci. USA **104**, 5268–5273 (2007)
70. He, M., Herr, A.E.: Automated microfluidic protein immunoblotting. Nat. Protoc. **5**, 1844–1856 (2010)
71. Bottenus, D., Jubery, T.Z., Ouyang, Y., Dong, W.-J., Dutta, P., Ivory, C.F.: 10000-fold concentration increase of the biomarker cardiac troponin I in a reducing union microfluidic chip using cationic isotachophoresis. Lab Chip **11**, 890–898 (2011)
72. Smejkal, P., Bottenus, D., Breadmore, M.C., Guijt, R.M., Ivory, C.F., Foret, F., Macka, M.: Microfluidic isotachophoresis: a review. Electrophoresis **34**, 1493–1509 (2013)
73. MICROBIAL FACTSHEET SERIES: *Staphylococcus aureus*. https://www.fsai.ie/staphylococcusaureus.html. Accessed 4 Sept 2021
74. Hennekinne, J.-A., De Buyser, M.-L., Dragacci, S.: Staphylococcus aureus and its food poisoning toxins: characterization and outbreak investigation. FEMS Microbiol. Rev. **36**, 815–836 (2012)
75. König, C., Simmen, H.P., Blaser, J.: Bacterial concentrations in pus and infected peritoneal fluid–implications for bactericidal activity of antibiotics. J. Antimicrob. Chemother. **42**, 227–232 (1998)
76. Ghias, W., Sharif, M., Yazdani, F.A., Rabbani, M.: Isolation and identification of Methicillin and Vancomycin resistance *Staphylococcus aureus* from pus samples of injured skin patients in Lahore Pakistan. Biomed. Lett. **2**, 103–112 (2016)
77. Lien, K.-Y., Lee, G.-B.: Miniaturization of molecular biological techniques for gene assay. Analyst **135**, 1499–1518 (2010)